Implementation of MPPT Enabled SPV Fed Fully Controlled PMSM Drive Using DC-DC Cascaded Boost Converter and Z-Source Inverter

Tamaghna Das, Sarbojit Mukherjee and Prasanna Biswas

Published online: 27 November 2023.

Submit your article to this journal: ↗

Article views: ↗

View related articles: ↗

View Crossmark data: ↗

Full Terms & Conditions of access and use can be found at https://ijmit.org/mission.php

Implementation of MPPT Enabled SPV Fed Fully-Controlled PMSM Drive Using DC-DC Cascaded Boost Converter and Z-Source Inverter

Tamaghna Das, Sarbojit Mukherjee and Prasanna Biswas

Department of Electrical Engineering, RCC Institute of Information Technology, Kolkata, India

ABSTRACT

This paper represents two-stage Permanent Magnet Synchronous Machine (PMSM) drive, consisting of a multistage DC-DC boost converter followed by a Z-source Inverter (ZSI), suitable for MPPT enabled Solar-Photovoltaic (SPV) based application. Available low voltage DC can be boosted up by the multistage DC-DC converter through which high gain can be achieved. A traditional ZSI is further used in the design to produce the three-phase AC power. The open loop speed control of the PMSM drive can be implemented by duty cycle control of the DC-DC converter. Furthermore, an incremental conductance (IC) based MPPT is implemented for extraction of maximum available solar power. The total system is simulated in the MATLAB Simulink and verification of the voltage and current characteristics of the different converters are carried out. Performance analysis of the PMSM drive is also carried out.

1. INTRODUCTION

Due to constant reduction in solar price, renewable-energy based systems like standalone water pump, electric vehicle charging station, etc. are getting popular day-by-day. Photovoltaic (SPV) is the leading option for renewable energy systems. Since the efficiency of commercial solar cells is still less than 23%, it is very important to extract the maximum solar power in an optimal way. Low maintenance and less installation time for customized power rated applications are some of the technical and economic reasons that encourage the installation of renewable-energy based systems [1].

The maximum output of an SPV array at a given irradiance and temperature occurs only at a given voltage (V_{mp}) and current (I_{mp}) of the SPV array [2]. A maximum power point tracking (MPPT) controller is used to determine the control signal required to generate the gate pulse corresponding to the maximum power of the SPV array. MPPT controllers work with any of the following algorithms: perturbation and observation (P&O), incremental conductance, open-circuit voltage, short-circuit current, parasitic capacitance, curve fitting, fuzzy logic control, artificial neural networks, and optimization control [3, 4]. Among them, the P&O method [5] and the incremental conductivity method are widely used.

For most renewable-energy based applications, a two stage DC-AC power conversion topology is preferable, i.e., a DC-DC converter followed by a DC-AC converter. Variety of DC converters [2, 6–10] are used by different researchers for SPV applications but high gain DC-DC converters serve the best purpose. However, reduced efficiency due to poor reverse recovery and considerable conduction loss in the power devices during large duty

cycle applications, make these unsuitable for many applications. Some solutions have been provided with transformer or coupled-inductor based designs to attain high conversion gain with reduced duty ratio based operation [11–13].

Again, a voltage overshoot, observed due to the leakage inductance in a transformer or couple inductor, reduces the overall system efficiency. Further, using some non-dissipative snubber circuit or active and passive clamp circuit, the minimization of the voltage overshoot can be minimized. Besides, some switched capacitor, switched inductor based non-isolated topologies are also prescribed for achieving high conversion gain [14–16]. But all this topology enhancement largely increases design complexity as well as the overall cost of the system. The high conversion ratio can also be achieved by implementing cascaded structures [17]. Multiple boost cells are connected in cascaded mode which require multiple control circuit and component. But again, cascaded converter can also be realized using integrating multiple boost converter with a single control circuit [18].

In recent years, the application of Permanent Magnet Synchronous Machine (PMSM) has been growing immensely, especially in the field of renewable-energy based systems due to the improvement in the permanent magnet technology [19]. Highly reliable performance with better efficiency and noiseless operation with long life has made this a good replacement for the existing drive. A conventional Voltage Source Inverter (VSI) is preferably used as DC-AC power conversion. But it is only capable of generating voltages lower than the DC grid voltage. Besides that, for high frequency switching application shoot-through may cause a considerable issue. This problem can be eliminated by using a Z-Source Inverter

(ZSI) where shoot-through can be used as a boost mode to generate greater output voltage [20–23].

In this paper an MPPT-based solar-power fed two-stage PMSM drive is developed using a cascaded DC-DC boost converter and a Pulse Width Modulated (PWM) Z-source Inverter. The total system is simulated in MATLAB Simulink and its different characteristics have been analyzed.

2. PROPOSED TOPOLOGY

Fig-1 represents the overall scheme of the proposed work. A two-stage power conversion using a DC-DC cascaded boost converter and a DC-AC Z-source inverter is used for the PMSM drive.
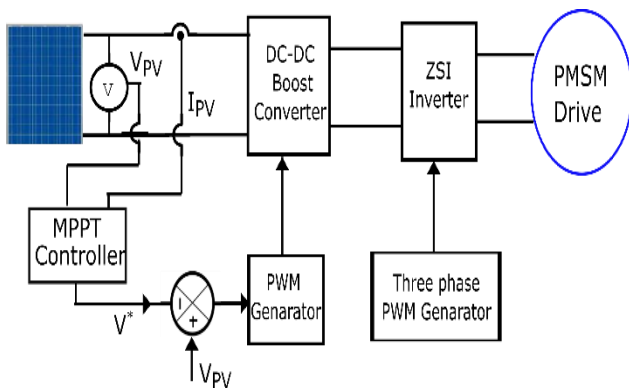
Fig. 1: Proposed diagram of overall scheme

A. Maximum Power Point Tracking and its Algorithm

To extract maximum power from solar photovoltaic arrays, the concerned system requires to operate at the maximum power point (MPP). Temperature and irradiance are the two main factors that affect the MPP. Hence, determining the value of the MPP is a major point which is primarily through three different methods, viz., Perturb & Observe (PO) method, Incremental Conductance (IC) method and the Three-Point method. Out of the options mentioned, the IC method has both, theoretically and experimentally, turned out to be the most efficient.

(a)

(b)
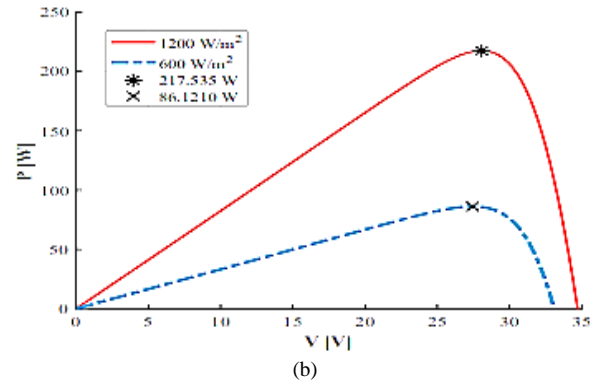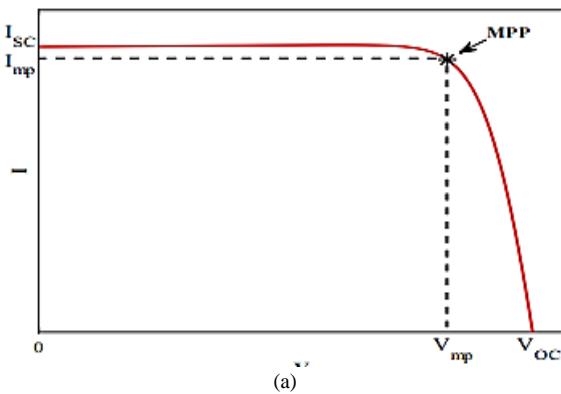
Fig-2: (a): I-V Characteristic of typical SPV array
(b) Change in MPP with change in irradiance
[24]

The I-V characteristic curve of a typical PV array is shown in Fig-2(a). On this curve, there exists only a single point where the product of the current and the voltage is maximum and is known as the MPP. While, Fig-2(b) shows the change of the MPP with change in irradiance.
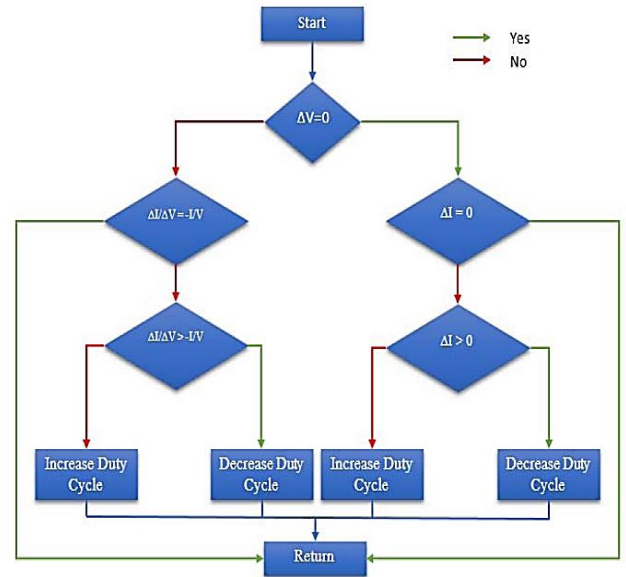
Fig-3: MPPT algorithm incorporating Incremental Conductance [24]

In the incremental conductance (IC) method, the MPP is found by comparing the incremental conductance with the instantaneous conductance. It can be analyzed that the derivative of power with respect to voltage at the MPP must be zero. Hence-

$$\frac{dP}{dV} = \frac{d}{dV}(VI) = 1 + V\frac{dI}{dV} = 0 \qquad (1)$$

By choosing a very small step size, i.e.,

$$\frac{\Delta I}{\Delta V} \approx \frac{dI}{dV} \qquad (2)$$

Therefore, the condition for the MPP-

$$\frac{\Delta I}{\Delta V} = -\frac{I}{V} \qquad (3)$$

Equation-(3) reveals that the operating point is at the MPP if the value of incremental conductance is equal to the negative of the instantaneous conductance. Therefore, if the incremental conductance is lesser than the instantaneous conductance, the operating point needs to shift left by increasing the operating voltage, to achieve the MPP, and vice versa. Fig-3 shows a flowchart depicting the working principle of the incremental conductance algorithm.

B. DC-DC Three-Stage Boost Converter

A DC-DC boost converter, shown in Fig-3(a), converts a small, fixed DC voltage to a boosted DC voltage. There are two modes of operation of the converter: (i) In the switch-on state, shown in Fig-3(b), the inductor L_1 provides a short-circuit path and charges while the capacitor C_1 discharges across the load; (ii) In the switch-off state, shown in Fig-3(c), the inductor discharges and the boost operation occurs as the voltage across the load is the sum of V_{in} and V_{L1}. In the meantime, capacitor C_1 also gets charged.
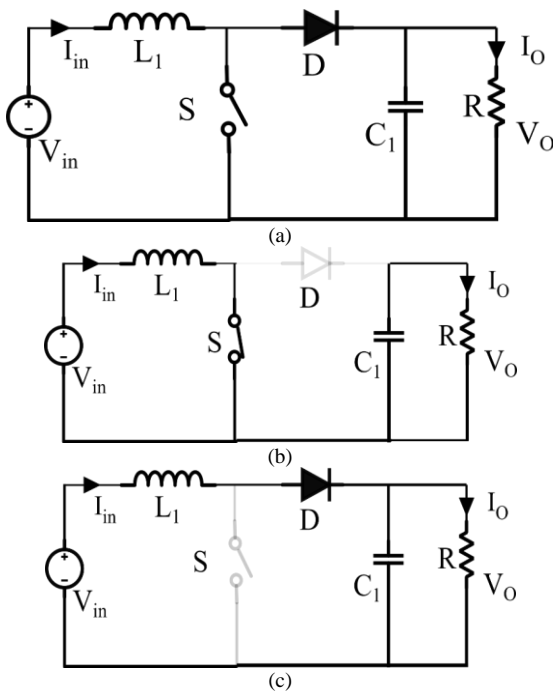
Fig-3: (a) Basic circuit diagram of Elementary Boost Converter; (b) On-state equivalent circuit; (c) Off-state equivalent circuit

Now, for an elementary DC-DC Boost Converter, if V_{in} be the input voltage and T be the total time period, then output voltage of the chopper used in our case,

$$V_o = \frac{1}{1-k}V_{in} \tag{4}$$

and the voltage transfer gain,

$$G = \frac{V_o}{V_{in}} = \frac{1}{1-k} \tag{5}$$

where, k is the duty-cycle of the pulse generator.

Now, to further boost a voltage, multiple stages of this elementary boost converter can be used in cascaded format. In our case, a three-stage boost was implemented to obtain the desired voltage. The circuit diagram and equivalent circuits during switch-on and switch-off states for the 3-Stage DC-DC Boost Converter are shown in Fig-4(a), 4(b) and 4(c) respectively.

In this case, capacitor C_1 and C_2 are charged to V_1 and V_2 respectively during the switch-off period. V_1 and V_2 are calculated to be,

$$V_1 = \frac{1}{(1-k)}V_{in} \tag{6}$$

$$V_2 = \left(\frac{1}{1-k}\right)^2 V_{in} \tag{7}$$

The voltage across capacitor C_3 is increased to V_0. Therefore, the output voltage is calculated to be:

$$V_o = \frac{1}{1-k}V_2 = \left(\frac{1}{1-k}\right)^2 V_1 = \left(\frac{1}{1-k}\right)^3 V_{in} \tag{8}$$

while the voltage transfer gain,

$$G = \frac{V_o}{V_{in}} = \left(\frac{1}{1-k}\right)^3 \tag{9}$$
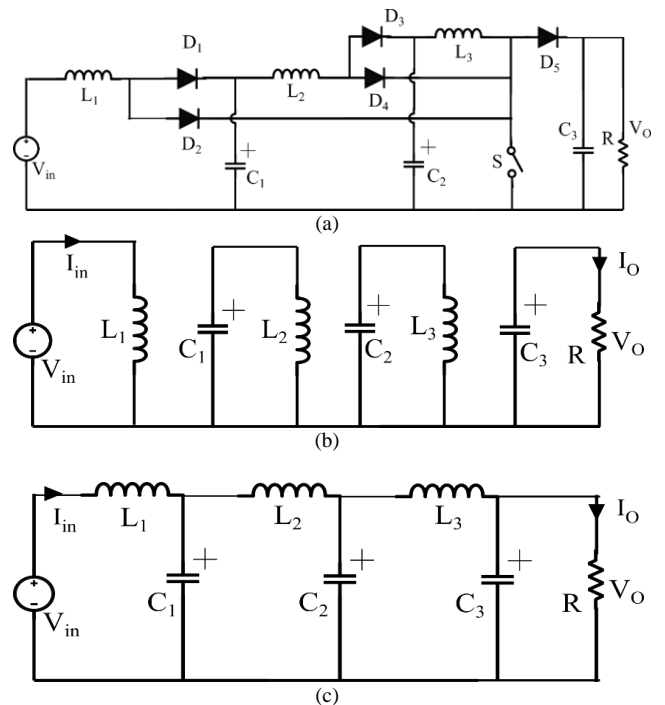
Fig-4: (a) Basic circuit diagram of 3-Stage Boost Converter;
(b) On-state equivalent circuit;
(c) Off-state equivalent circuit

C. Pulse-width-modulated ZSI

Traditional VSI [5] and CSI cannot operate in buck-boost mode. Their components are vulnerable to permanent damage by high current or voltage stresses. Dead time for VSI and overlap time for CSI can cause waveform

distortion. The power circuit topology of VSI and CSI are not interchangeable.

(a)

(b)
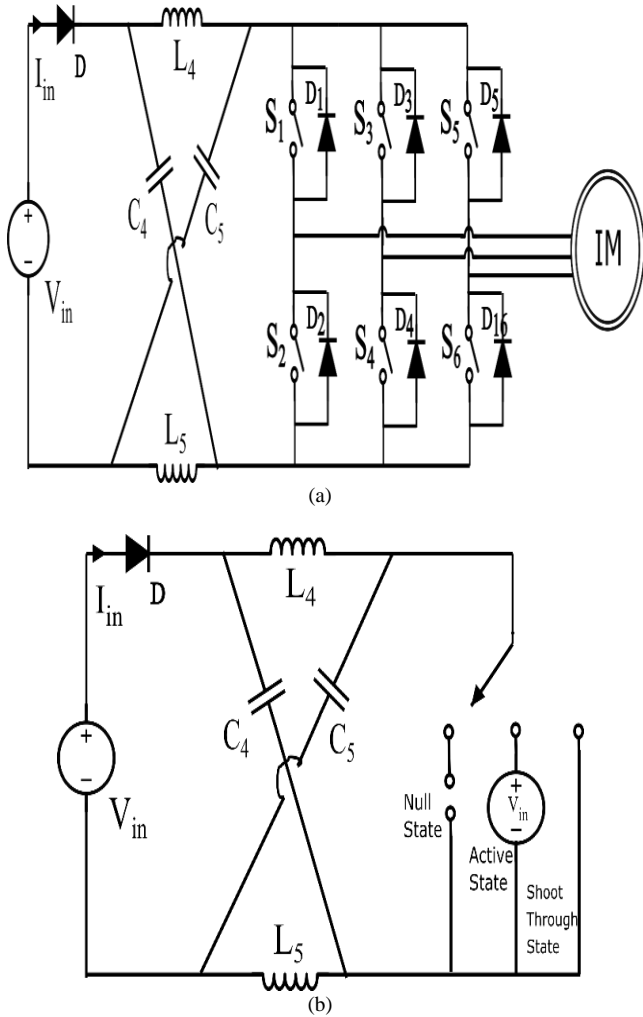
Fig-5: (a) Basic circuit diagram of a Z-Source Inverter; (b) Three modes of operation of ZSI- Null mode, Active mode and Shoot-through mode

A ZSI, shown in Fig-5(a), that comprises of two small inductors and capacitors, arranged in a specific structure, eliminates almost all the problems that arise in a conventional VSI or CSI. The network acts as a second-order filter to suppress voltage ripples, while the inrush current and harmonics in the current can be reduced via the inductors. The ZSI can operate in either of three modes as shown in Fig-5(b).

1. *Active Mode:* The battery voltage is given to the inverter and the load; can be achieved in six different ways.
2. *Null Mode:* The battery voltage appears directly across the load and the inverter is open circuited; can be achieved in two different ways.
3. *Shoot-through Mode:* The load terminals are short-circuited by the conduction of both switches in one or more legs; can be achieved in seven different ways; mode unavailable in traditional inverters.
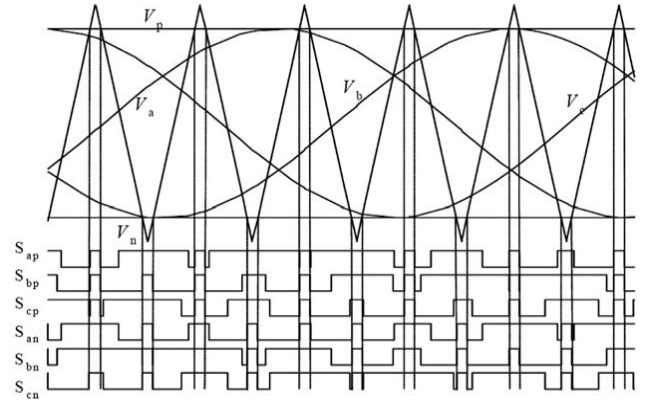
Fig-6: Simple Boost Pulse Width Modulated Gate Firing Signals

In our case, as shown in Fig-6 [25], the Simple-Boost PWM technique is used to configure the gate-firing pulses. This technique makes use of four different signals- a 3-phase sinusoidal waveform, a continuous triangular wave and two straight DC reference signals. Each phase of the sine wave (V_a, V_b and V_c), which corresponds to each leg of the inverter, is compared with the triangle wave (V_t) individually. For every case, where the magnitude of the sinusoid is greater than that of the triangle, the upper switch of the corresponding leg is turned on and the lower turned off. Reverse occurs when the magnitude of the triangle is smaller than that of the sinusoid. Furthermore, the two straight DC lines, V_p and V_n, are used as upper and lower shoot-through lines respectively. Whenever the triangular reference signal is greater than V_p or lesser than V_n, shoot-through occurs.

In case of SBPWM operating technique of ZSI, we know that voltage across the LC-impedance part,

$$V_{int} = BV_{DC} \tag{10}$$

where B and d are known as the Boost Factor and duty cycle respectively, the values are given as:

$$B = \frac{1}{(1-2d)} \tag{11}$$

where,

$$d = \frac{T_{shoot}}{T_S} \tag{12}$$

(T_s= Total switching time period; T_{shoot} = Shoot-through time; T_{active} = Active-state time; $T_s = T_{active} + T_{shoot}$)
Now, we know, output voltage of an inverter,

$$V_{AC} = M \frac{V_{int}}{2} \tag{13}$$

where, V_{int} is the voltage across the LC-impedance part of the inverter and M is the modulation index given as:

$$M = \frac{E_R}{E_C} \tag{14}$$

(E_R = Gating rectangular signal; E_C = Triangular carrier wave signal)
Therefore, the output voltage of the ZSI,

$$V_{AC} = MB \frac{V_{DC}}{2} \tag{15}$$

$$V_{AC} = G \; \frac{V_{DC}}{2} \qquad (16)$$

where,

$$G = MB \qquad (17)$$

and G is known as the Voltage Gain of the ZSI.

Hence, any desired output voltage of the inverter can be obtained by properly selecting the values of M (which can be controlled by the values of E_R and E_C) and B (which depends on the duty cycle d) without the need of changing the input DC supply to the inverter, V_{DC}, which, in our case is the output of the 3-Stage Boost Converter, V_o).

3. DESIGN CONSIDERATIONS

Designing of inductor L_1: One of the primary components of this three-stage boost converter is the inductor L_1. Initially, the inductor gets charged up during on-time and discharges during the off-time. The value of the inductor can be calculated from the Equation-(18)

$$L_1 = \frac{V_{in}}{\Delta i_{L_1}} kT \qquad (18)$$

So, the value of the inductor is primarily dependent on the duty cycle of the operating switch signal and the magnitude of the ripple current. Considering the input voltage as a constant value, the change in the inductor value, due to variation of duty cycle (30% to 75%) and current ripple (2% to 10%), can be observed in Fig-7. It is seen that the value of the inductance is reduced as the current ripple increases. Therefore, a very small current ripple in the inductor may result in a large value of the inductance. Furthermore, as the value of inductance increases with the duty cycle, the maximum value of the duty cycle is bound within 75% to limit the inductor value up to 10mH.

Inductor Value (L₁)
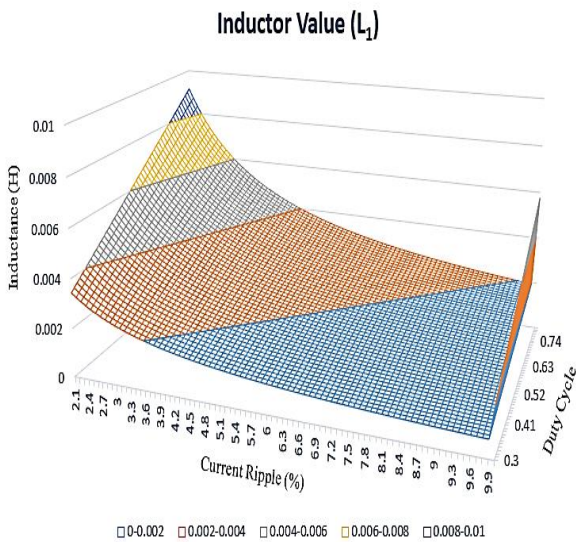
Fig-7: Variation of inductance of L_1 with change in duty cycle and current ripple

Designing of inductors L_2 and L_3: Similarly, the values of inductors L_2 and L_3 are also calculated using Equation-(19)

and Equation-(20) respectively. For both the cases, the maximum operating duty cycle is bound up to 75%. The variations of the values of L_2 and L_3 with duty cycle and current ripple are shown in Fig-8 and Fig-9.

$$L_2 = \frac{V_1}{\Delta i_{L_2}} kT \qquad (19)$$

$$L_3 = \frac{V_2}{\Delta i_{L_3}} kT \qquad (20)$$

Inductor Value (L₂)
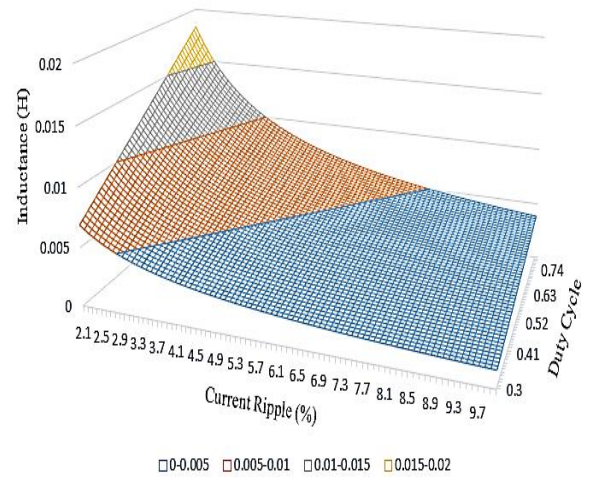
Fig-8: Variation of inductance of L_2 with change in duty cycle and current ripple

Inductor Value (L₃)
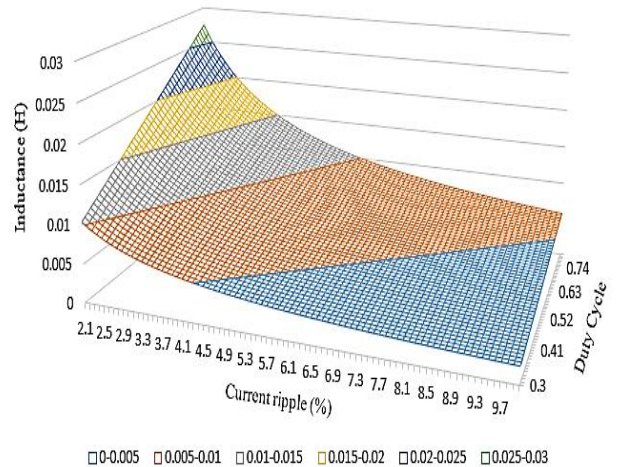
Fig-9: Variation of inductance of L_3 with change in duty cycle and current ripple
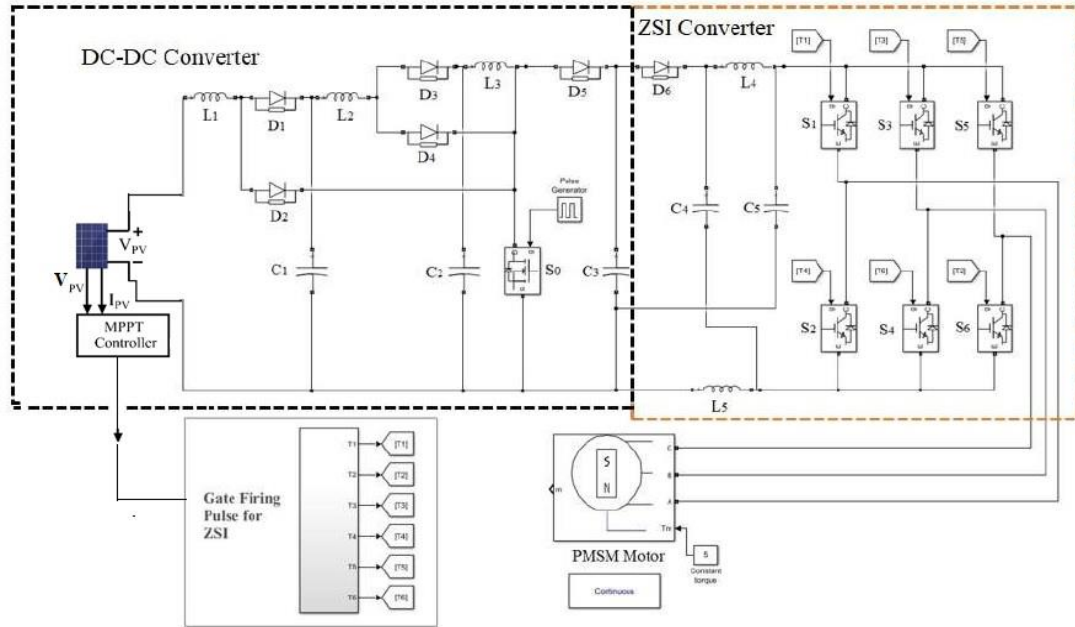
Fig-10: Simulation diagram of proposed topology

4. SIMULATION AND RESULTS

To demonstrate the performance of the above proposed topology, a MATLAB Simulink model of the entire system was developed, as shown in Fig-10.

The 3kW DC-DC converter was designed for an input voltage of 48V. Further, a cascaded connection of a DC-DC boost converter and a Z-source inverter is made. Six MOSFET switches, S_1-S_6, used in a three-leg configuration, represent three different phases. Besides that, two capacitors, C_4 and C_5 and two inductors L_4 and L_5 forms the Z-topology of the inverter. A Pulse Width Modulated (PWM) signal of frequency 20 kHz is developed with a modulation index of 1 using a separate subsystem and transferred to the ZSI. Finally, a round rotor type three-phase PMSM drive is connected to the inverter. The details of the components are provided in Table-1.

	C_3	2uF
	C_4 and C_5	2mF
Operating Frequency	f_{dc}	5kHz
	f_{inv}	20kHz
PMSM (Round Rotor)	R_{rotor}	0.36Ω
	$R_{inductance}$	1.67Ω
	Pole pair	4

The SPV output voltage and power at MPP for different irradiance levels are shown in Fig-11(a) and Fig-11(b) respectively. For an irradiance of 1000W/m², the photovoltaic array outputs approximately 160W at an operating voltage of around 55V. Even when the irradiance level falls to half the previous value, to 500W/m², the SPV still operates at about 100W-40V, owing to the incorporation of the incremental conductance technique. Thus, the IC-MPPT control exploits the SPV at maximum. Fig-12 shows the DC-DC boost converter output power for varying input from the photovoltaic array and almost no power-loss is realized.

Table. 1 Component Details

Parameter		Element	Value
Panel Specification	Input panel power	P_{pv}	175W
	Open circuit voltage	V_{oc}	53.99V
	Voltage at MPP	V_{MPP}	46.63V
	Short circuit current	I_{sc}	4.17A
	Current at MPP	I_{MPP}	3.78A
	Temp coefficient of V_{oc}	V_{oc}	-0.3616 %/ºC
	Temp coefficient of I_{sc}	I_{sc}	0.0415 %/ºC
Rated output voltage (DC-DC Converter)		V_o	250V
Inductance		L_1	10mH
		L_2	20mH
		L_3	30mH
		L_4 and L_5	1mH
Capacitance		C_1	110uF
		C_2	120uF

Fig-11: For varying irradiance at maximum power point (MPP):
(a) SPV output voltage; (b) SPV output power
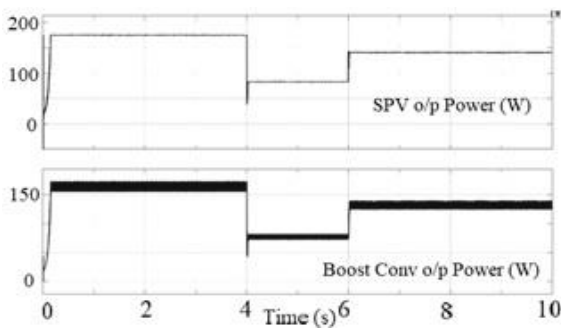
Fig-12: DC-DC Converter output power for varying input from SPV

Fig-13 shows the variation of output voltage and current with respect to 50% duty cycle of the power switch for an input voltage of 48V. An output voltage of 248V with 2.5V voltage ripple and output current 12.4A with 0.2 current ripple is observed with 50% duty cycle. In Fig-14, the gain of the converter, i.e., output voltage is shown against the input voltage.

Voltages across C_1 and C_2 are shown in the Fig-15. Fig-16 shows the charging and discharging of the three converter inductor currents with peaks of 101.5A, 51A and 25.5A respectively across L_1, L_2 and L_3 respectively.
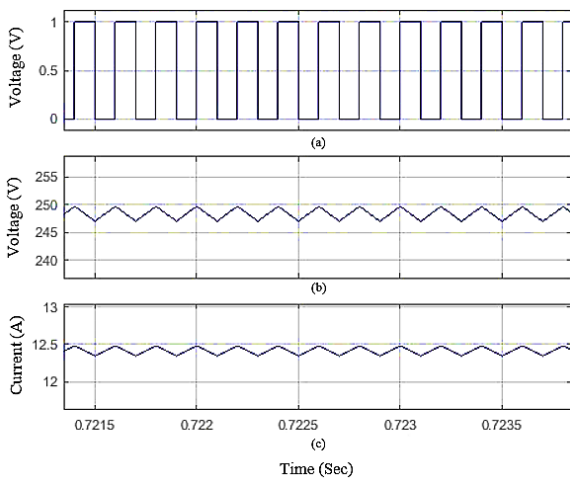
Fig-13: DC-DC Converter parameters with 50% Duty Cycle:
(a) Gate Voltage (b) Output Voltage (c) Output Current
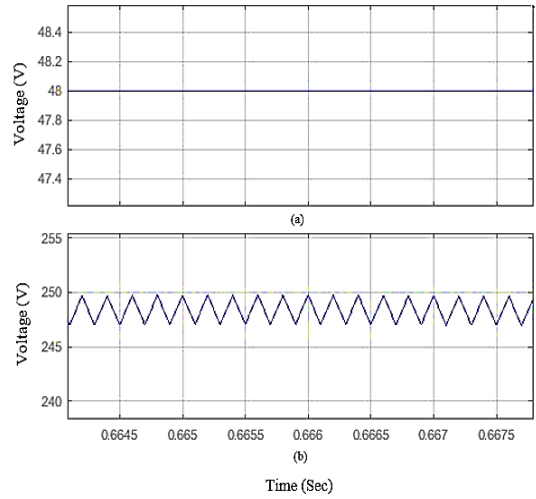
Fig-14: DC-DC Converter: (a) Input Voltage (b) Output Voltage
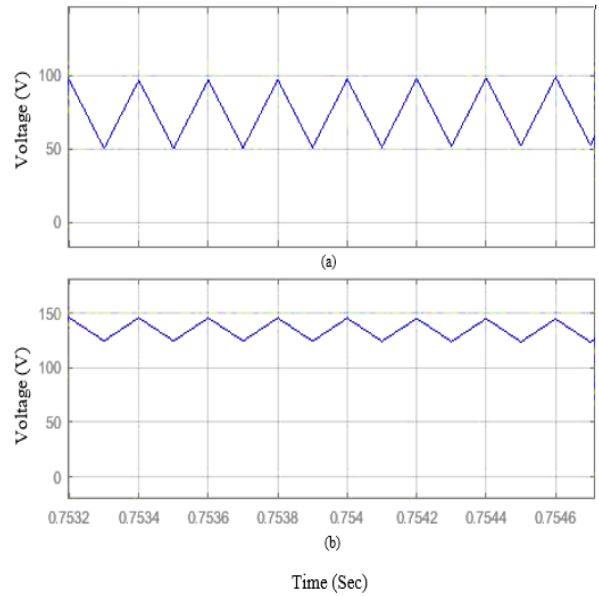
Fig-15: Different Capacitor Voltages of DC-DC
Converter: (a) C_1 (b) C_2
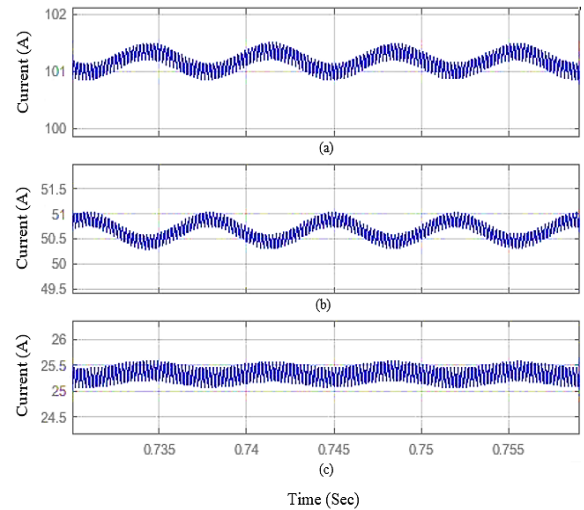
Fig-16: Different Inductor Currents of DC-DC
converter: (a) L_1 (b) L_2 (c) L_3
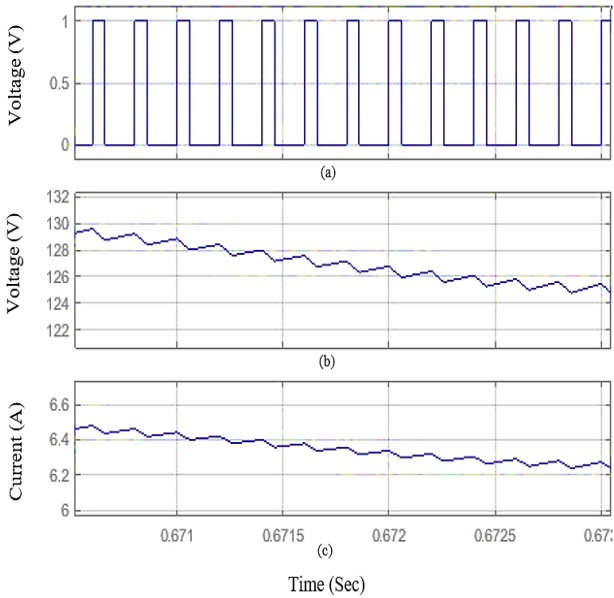
Fig-17: DC-DC Converter parameters with 30% Duty Cycle:
(a) Gate Voltage (b) Output Voltage (c) Output Current

Output characteristics of the DC-DC converter are shown in Fig-17 for duty of 30%. An average output voltage of 125V with 1V voltage ripple and an average output current of 6.3A with 0.1A current ripple are seen. The output of the inverter phase voltage is shown in the Fig-18. Finally, the angular velocity, torque, and the current of the PMSM drive is represented by Fig-19. A very low Total Harmonic Distortion (THD) is achieved and shown in Fig-20.
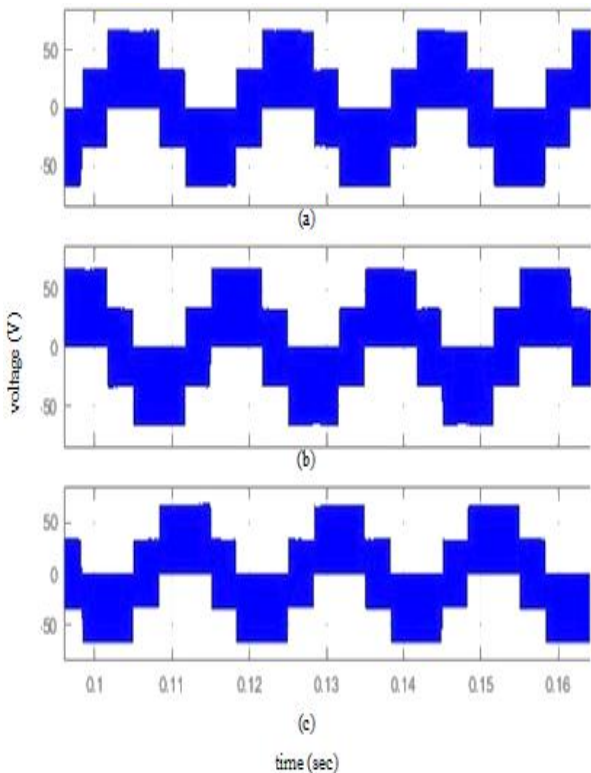
Fig-18: ZSI output phase voltages
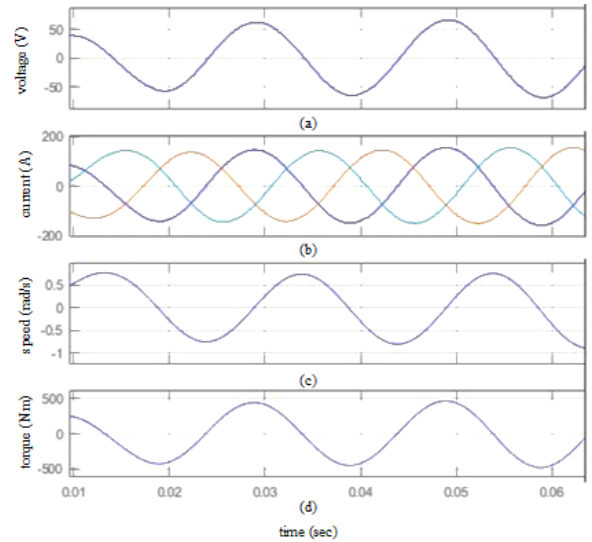
Fig-19: (a) Voltage across PMSM (b) Stator Current of PMSM (c) Rotor Speed of PMSM (d) Torque Waveform of PMSM
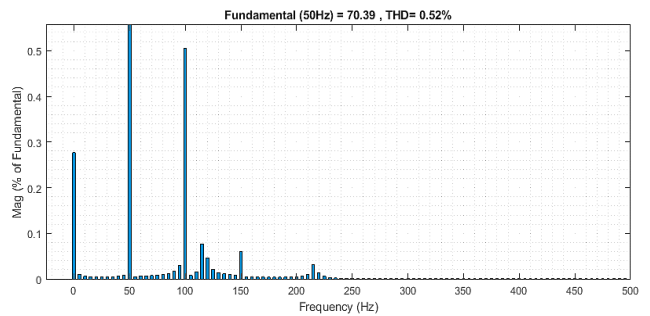
Fig-20: THD of the ZSI output Voltage

A comparative analysis of the proposed converter has been shown in Table-2. A boost interleaved buck-boost DC-DC converter with single-phase VSI is proposed in [26]. Besides, a switched linear topology based high gain dc-dc converter is proposed in [27] and a dual input dc-ac converter along with a high gain step up dc-dc converter is proposed in [28]. The gain of the DC-DC converter used in the proposed topology is better the topology proposed in [26, 27]. As the Z-Source Inverter is used in the proposed topology, reduction in the voltage and current stress in the active power switches can be achieved compared to all the other proposed converters. Besides that, better harmonics reduction is also observed in the proposed converter compared to [27, 28]. No. of active and passive switches used in the proposed converter is also less, resulting in a more compact overall design and a reduced development cost.

5. CONCLUSION

This paper represents a two stage PMSM drive based on a DC-DC and a DC-AC converter. The salient features of the converter can be described as
Successful implementation of MPPT for maximum power extraction.

- Successfully reduce the inductor current ripple in DC-DC multilevel converter.

- Design the MPPT fed Z-source inverter and implementation of modulation index control.
- Achieved minimization of THD in inverter output voltage.

A positive output cascaded boost DC-DC converter is used where minimum number of active switches are required. Besides, a PWM controlled Z- Source inverter is used to convert the power and transfer it to the PMSM drive. A change in the duty cycle, from 30% to 75%, is introduced in the DC converter and the variation of output voltage, from 130V to 250V is verified through simulation. Finally, the characteristics of the PMSM are also studied. In future this topology can be realized replacing the DC battery with solar-photovoltaic cells as the input source. An MPPT controller can also be introduced along with PWM controller for maximum power extraction.

Table. 2 Comparative Analysis

	Parameters		[26]	[27]	[28]	**Proposed Topology**
DC-DC Converter	Type		Buck-Cascaded Buck-Boost Interleaved with H-bridge unfolding circuit	Switched-Inductor Linear System Model-based Multicell I4SL-Boost	High Step-up/down	**3-Stage Cascaded Boost**
	Gain		1.37(Max Value)	3.5	6.5	**5-7**
	Operating Frequency (Hz)		NA	50kHz	100kHz	**5k**
	Power Rating		300W	50W<	1KW	**3KW**
	Ports		Two	Two	Three	**Two**
DC-AC Converter	Type		Single-phase Step-Up/Down VSI	Single-phase Traditional VSI	Single-phase Dual-input VSI	**Three-phase ZSI**
	Bidirectionality		Yes	No	No	**No**
	Voltage and current stress		High	High	High	**Low**
	Inverter Operating Frequency		20kHz	NA	20kHz	**20kHz**
General	Active and Passive Components Used	Capacitor	3	1	4	**5**
		Inductor	3	4	5	**5**
		Active and Passive Switches	8	11	12	**7**
	Switching losses		Low	High	High	**Medium**
	Renewable Energy Applications		Yes	Yes	Yes	**Yes**
	THD Minimization		Good	NA	Medium	**Very Good**

REFERENCES

1. Eltawil MA, Zhao Z (2010) Grid-connected photovoltaic power systems : Technical and potential problems — A review. 14:112–129. https://doi.org/10.1016/j.rser.2009.07.015
2. Mukherjee S, Saha SS, Chowdhury S (2021) Design of duty-ratio and phase-shift control circuits for MPPT of SPV Source using ZV-ZCS PSFB Converters. In: Proceedings of 4th International Conference on 2021 Devices for Integrated Circuit, DevIC 2021. IEEE, pp 555–559
3. Mukherjee S, Saha SS, Chowdhury S (2023) Battery Integrated Three-Port Soft-Switched DC-DC PSFB Converter for SPV Applications. IEEE Access 11:62472–62483. https://doi.org/10.1109/ACCESS.2023.3287149
4. Joshi P, Arora S (2017) Maximum power point tracking methodologies for solar PV systems – A review. Renewable and Sustainable Energy Reviews 70:1154–1177. https://doi.org/10.1016/j.rser.2016.12.019
5. Banerjee D, Mukherjee S, Dhar R (2021) Inverter with MPPT Technique. Springer Singapore
6. Khosroshahi AE, Wang L, Dadashzadeh H, et al (2019) A Two-Stage Coupled-Inductor-Based Cascaded DC-DC Converter with a High Voltage Gain. 2019 IEEE Canadian Conference of Electrical and Computer Engineering, CCECE 2019 1–5. https://doi.org/10.1109/CCECE.2019.8861768
7. He L, Zheng Z, Guo D (2018) High Step-Up DC-DC Converter with Active Soft-Switching and Voltage-Clamping for Renewable Energy Systems. IEEE Transactions on Power Electronics 33:9496–9505. https://doi.org/10.1109/TPEL.2018.2789456
8. Singh S, Swain SC, Dash R, Roy P (2017) Current control strategies for SPV grid interconnection based on artificial neural network. 2017 Innovations in Power and Advanced Computing Technologies, i-PACT 2017 2017-Janua:1–5. https://doi.org/10.1109/IPACT.2017.8245208
9. Mahadik VS, Katti PK (2018) Pumping with Multifunction Converter. 2018 International Conference on Power Energy, Environment and Intelligent Control (PEEIC) 392–397, 5195
10. Singh Y, Hussain I, Singh B, Mishra S (2016) Improved adaptive detection based control of grid integrating solar energy system. India International Conference on Power Electronics, IICPE 2016-Novem: https://doi.org/10.1109/IICPE.2016.8079357
11. Wu TF, Lai YS, Hung JC, Chen YM (2008) Boost converter with coupled inductors and buck-boost type of active clamp. IEEE Transactions on Industrial Electronics 55:154–162. https://doi.org/10.1109/TIE.2007.903925
12. Alghaythi ML, O'Connell RM, Islam NE, et al (2020) A High Step-Up Interleaved DC-DC Converter with Voltage Multiplier and Coupled Inductors for Renewable Energy Systems. IEEE Access 8:123165–123174. https://doi.org/10.1109/ACCESS.2020.3007137
13. Kumar N, Veerachary M (2017) Analysis and design of high gain fourth-order boost converter. IEEE International Conference on Power Electronics, Drives and Energy Systems, PEDES 2016 2016-Janua:1–6. https://doi.org/10.1109/PEDES.2016.7914409
14. Axelrod B, Berkovich Y, Ioinovici A (2008) Switched-

capacitor/switched-inductor structures for getting transformerless hybrid DC-DC PWM converters. IEEE Transactions on Circuits and Systems I: Regular Papers 55:687–696. https://doi.org/10.1109/TCSI.2008.916403

15. Chung HSH, Chow WC, Hui SYR, Lee STS (2000) Development of a switched-capacitor dc-dc converter with bidirectional power flow. IEEE Transactions on Circuits and Systems I: Fundamental Theory and Applications 47:1383–1389. https://doi.org/10.1109/81.883334

16. Azar MA, Shahir FM, Taher B (2018) New single switch topology for non-isolated boost DC-DC converter based on voltage-lift technique. Proceedings - 2018 IEEE 12th International Conference on Compatibility, Power Electronics and Power Engineering, CPE-POWERENG 2018 1–6. https://doi.org/10.1109/CPE.2018.8372515

17. Huber L, Jovanovic MM (2000) Design approach for server power supplies for networking applications. Conference Proceedings - IEEE Applied Power Electronics Conference and Exposition - APEC 2:1163–1169. https://doi.org/10.1109/apec.2000.822834

18. Zhu M, Wang T, Luo FL (2012) Analysis of voltage-lift-type boost converters. Proceedings of the 2012 7th IEEE Conference on Industrial Electronics and Applications, ICIEA 2012 214–219. https://doi.org/10.1109/ICIEA.2012.6360725

19. Antonello R, Carraro M, Costabeber A, et al (2017) Energy-efficient autonomous solar water-pumping system for permanent-magnet synchronous motors. IEEE Transactions on Industrial Electronics 64:43–51. https://doi.org/10.1109/TIE.2016.2595480

20. Peng FZ (2002) Z-source inverter. Conference Record - IAS Annual Meeting (IEEE Industry Applications Society) 2:775–781. https://doi.org/10.1002/047134608x.w8348

21. Battiston A, Miliani EH, Martin JP, et al (2014) A control strategy for electric traction systems using a PM-motor fed by a bidirectional Z-source inverter. IEEE Transactions on Vehicular Technology 63:4178–4191. https://doi.org/10.1109/TVT.2014.2312434

22. Dubey M, Sharma S, Saxena R (2018) Solar Power Based Water Pump Employing Z-Source Inverter for PMSM Drive. India International Conference on Power Electronics, IICPE 2018-Decem:1–5. https://doi.org/10.1109/IICPE.2018.8709405

23. Mukherjee S, Mal C, Yadav G (2022) Design of MPPT DC-DC Converter Fed Ripple Switch Inductor Quasi-ZSI with Different Control Methods For Renewable Energy Application. Neuro Quantology 20:4715–4726. https://doi.org/10.14704/nq.2022.20.9.NQ44547

24. Bendib B, Belmili H, Krim F (2015) A survey of the most used MPPT methods: Conventional and advanced algorithms applied for photovoltaic systems. Renewable and Sustainable Energy Reviews 45:637–648. https://doi.org/10.1016/j.rser.2015.02.009

25. Shen M, Wang J, Joseph A, et al (2006) Constant boost control of the Z-source inverter to minimize current ripple and voltage stress. IEEE Transactions on Industry Applications 42:770–778. https://doi.org/10.1109/TIA.2006.872927

26. Chang CH, Chang EC, Cheng CA, Shen CL (2015) A step-up/down inverter implemented with the boost-interleaved buck-boost dc-dc converter. In: 2015 IEEE 2nd International Future Energy Electronics Conference, IFEEC 2015

27. Zhang G, Heng P, Yu S, et al (2021) Controllability Analysis and Verification for High-Order DC-DC Converters Using Switched Linear Systems Theory. IEEE Transactions on Power Electronics 36:9678–9688. https://doi.org/10.1109/TPEL.2021.3059259

28. Yang L, Peng J, Yang F, et al (2019) Single-Phase High-gain Bidirectional DC / AC Converter Based on High Step-up / step-down DC / DC Converter and Dual-input DC / AC Converter. 2019 IEEE 10th International Symposium on Power Electronics for Distributed Generation Systems (PEDG) 554–559

AUTHORS

Tamaghna Das received his B.Tech. degree in Electrical Engineering in 2023 from RCC Institute of Information Technology, affiliated to Maulana Abul Kalam Azad University of Technology (MAKUT), West Bengal, India. He has previously served as a Service Engineer for PLC, VFD, HMI, etc. at Yuva Solutions, Kolkata. Currently, he is working as a Programmer Analyst Intern in dot Net at Cognizant Technology Solutions. His research interests include power converter topologies, DC and AC, for renewable and PWM strategies.

Email: tamaghnadas.mi@gmail.com

Sarbojit Mukherjee (Member, IEEE) received his B.Tech. degree in Electrical Engineering from West-Bengal University of Technology, Kolkata, India, in 2009, and his M.Tech. degree in Electrical Engineering from Calcutta University, India, in 2011. He is currently pursuing his Ph.D. degree in Electrical engineering at Calcutta University, Kolkata, India. He has 12 years of teaching experience as a Lecturer and Assistant Professor. Since 2012, he has been working as an Assistant Professor in the Department of Electrical Engineering, RCC Institute of Information Technology, Kolkata, India. His current research interests include high-frequency dc-dc converter topology and control, and power converters in renewable generation.

Email: sarbo.1234@gmail.com

Prasanna Biswas received his B.Tech. degree in Electrical Engineering in 2023 from RCC Institute of Information Technology, affiliated to Maulana Abul Kalam Azad University of Technology (MAKUT), West Bengal, India. He is currently working as a Full-Stack Developer intern at Texcial Lite Pvt. Ltd. His research interests include power converter topologies for renewable energy sources and EV applications.

Email: probiswas82@gmail.com